

Supporting Information

Non-equilibrium Thermodynamics in Electrochemical Complexation of Li-Oxygen Porous Electrodes

Aashutosh N. Mistry,^{†1} Fernando Cano-Banda,[‡] Dickens Law,[§] Abel Hernandez-Guerrero^{‡2} and Partha P. Mukherjee^{†3*}

[†] Energy and Transport Sciences Laboratory (ETSL), School of Mechanical Engineering, Purdue University, West Lafayette, Indiana 47907, United States

[‡] Department of Mechanical Engineering, University of Guanajuato, Salamanca, Guanajuato 36885, Mexico

[§] Energy and Transport Sciences Laboratory (ETSL), Department of Mechanical Engineering, Texas A&M University, College Station, Texas 77843, United States

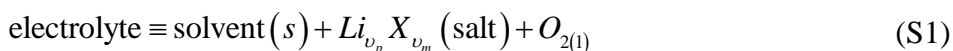
The mathematical details supplementing the electrochemical dynamics in the manuscript are presented here:

- S1. Concentrated Solution Theory for a Liquid Electrolyte containing Dissolved Oxygen
- S2. Reaction Kinetics with an Insulating Insoluble Reactant
- S3. Abstracting Porous Electrode Evolution upon Precipitation
- S4. Electrochemical Description of a Porous Evolving Electrode

S1. Concentrated Solution Theory for a Liquid Electrolyte containing Dissolved Oxygen

An electrolyte is prepared by mixing salts (containing the ions of interest, *e.g.*, Li^+ for lithium batteries) in solvents. At lower concentrations, each of the solute molecules behaves independently of each other. Such a state is known as the ‘*dilute solution limit*’ in literature. As the solute concentration increases, the solvation shells of neighboring species overlap and causes an increased hindrance to mobility (in addition to the solvent viscosity effect). In such a concentrated state, electrolyte transport is described by the ‘*concentrated solution theory*’¹⁻⁴.

The electrolyte transport description for Li-oxygen electrochemistry is more involved due to the presence of an extra solute species – dissolved oxygen, $O_{2(l)}$:



* Email: pmukherjee@purdue.edu

¹ ORCID: 0000 – 0002 – 4569 – 4975

² ORCID: 0000 – 0003 – 3540 – 7524

³ ORCID: 0000 – 0001 – 7900 – 7261

** ETSL moved to Purdue University in August 2017.

A common salt for Li-oxygen system is *LiTFSI* (Lithium bis(trifluoromethanesulfonyl)imide) that decomposes into Li^+ cation and *TFSI*⁻ anion upon dissolution in appropriate organic solvents (e.g., DME, DMSO etc.). The corresponding salt dissolution (assuming complete dissociation) is:



where ν 's are stoichiometric coefficients and z 's are ionic valences ($z_p = +1$ for Li^+). The electrolyte solutions are locally charge neutral, i.e.,

$$\nu_p z_p + \nu_m z_m = 0 \quad (S3)$$

If the dissolved salt concentration is c , equivalent ionic concentrations (after dissociation) are:

$$c = \frac{c_p}{\nu_p} = \frac{c_m}{\nu_m} \quad (S4)$$

and the charge neutrality statement (Eq. (S3)) can be alternatively written as:

$$c_p z_p + c_m z_m = 0 \quad (S5)$$

The chemical potential of the salt can be equivalently expressed as a combination of individual ionic electrochemical potentials:

$$\begin{aligned} \mu &= \nu_p \mu_p + \nu_m \mu_m \\ \therefore \mu &= \mu^0 + \nu RT \log(fc) \end{aligned} \quad (S6)$$

where the salt stoichiometric coefficient is:

$$\nu = \nu_p + \nu_m \quad (S7)$$

and f is a thermodynamic factor for the salt. The thermodynamic factor accounts for the activity of salt. In the dilute limit, all the dissociated ions partake in transport and $f \rightarrow 1$, while as the salt concentration increases, the thermodynamic factor value decreases. It can be shown that the salt thermodynamic factor relates to the individual ionic thermodynamic factors via the expression:

$$f^\nu = f_p^{\nu_p} f_m^{\nu_m} \quad (S8)$$

As the oxygen is sparingly soluble in the organic electrolytes (mM concentrations in contrast to M salt concentrations), its thermodynamic activity can be assumed to be unity ($f_o \rightarrow 1$) and the corresponding chemical potential can be expressed as:

$$\mu_o = \mu_o^0 + RT \log c_o \quad (S9)$$

In shorthand notation $o \equiv O_{2(l)}$. The chemical potential gradients for all the components forming an electrolyte are interrelated via the Gibbs-Duhem relation:

$$\begin{aligned} c_s \nabla \mu_s + c_p \nabla \mu_p + c_m \nabla \mu_m + c_o \nabla \mu_o &= 0 \\ \therefore c_s \nabla \mu_s + c \nabla \mu + c_o \nabla \mu_o &= 0 \end{aligned} \quad (S10)$$

Species transport in such a multi-component environment follows the Stefan – Maxwell relation, where D_{ij} 's represent binary diffusivities and N_i 's are species i fluxes:

$$-\frac{c_i c_\Sigma}{RT} \nabla \mu_i = \sum_{\substack{j \\ j \neq i}} \left(\frac{c_j N_i - c_i N_j}{D_{ij}} \right) \quad (\text{S11})$$

The total local concentration is $c_\Sigma = c_s + c_p + c_m + c_o$. For an electrolyte composed of four (solvent, anion, cation and neutral) species, there are ${}^4P_2 = 12$ binary diffusivities⁵, out of which only 6 are independent given the symmetric nature of binary diffusivity tensor ($D_{ij} = D_{ji}$). Also, given the Gibbs-Duhem relation, only three species fluxes are independent. The following mathematical formulation is in terms of solute fluxes, *i.e.*, the fluxes are expressed with respect to the solvent. The motion of solvent molecules represents the bulk flow of the electrolyte solution, with a velocity u_s with respect to a stationary frame of reference.

Cation (Li^+) flux:

$$-\frac{c_p c_\Sigma}{RT} \nabla \mu_p = \left(\frac{c_m N_p - c_p N_m}{D_{pm}} \right) + \left(\frac{c_o N_p - c_p N_o}{D_{po}} \right) + \left(\frac{c_s N_p - c_p N_s}{D_{ps}} \right) \quad (\text{S12})$$

Anion (X^{zm}) flux:

$$-\frac{c_m c_\Sigma}{RT} \nabla \mu_m = \left(\frac{c_p N_m - c_m N_p}{D_{pm}} \right) + \left(\frac{c_o N_m - c_m N_o}{D_{mo}} \right) + \left(\frac{c_s N_m - c_m N_s}{D_{ms}} \right) \quad (\text{S13})$$

Dissolved oxygen (O_2) flux

$$-\frac{c_o c_\Sigma}{RT} \nabla \mu_o = \left(\frac{c_p N_o - c_o N_p}{D_{po}} \right) + \left(\frac{c_m N_o - c_o N_m}{D_{mo}} \right) + \left(\frac{c_s N_o - c_o N_s}{D_{so}} \right) \quad (\text{S14})$$

where D_{pm} , D_{po} , D_{mo} , D_{ps} , D_{ms} , and D_{so} are the six independent binary diffusivities, and $N_s = c_s u_s$. Equations (S12) to (S14) implicitly express species fluxes N_p , N_m and N_o in terms of (electro-) chemical potential gradients. The potential gradients, in turn, relate to concentration gradients via expressions (S6) and (S9). In addition to the binary diffusivities, the thermodynamic factor is a physical property affecting the transport interactions. Thus, in the electrolyte (Eq. (S1)) transport in Li-oxygen system is characterized by seven transport properties (in contrast to four for a typical Li-ion electrolyte²). However, these seven fundamental properties are difficult to measure in a typical electrochemical experiment and are to be rearranged to obtain more meaningful properties. It should be noted that recent NMR experiments⁴ have tracked individual ions and can provide more direct estimates for binary diffusivities. Rearranging the expressions (S12) to (S14):

$$\left. \begin{aligned} N_p \left(\frac{c_m}{D_{pm}} + \frac{c_o}{D_{po}} + \frac{c_s}{D_{ps}} \right) - N_m \left(\frac{c_p}{D_{pm}} \right) - N_o \left(\frac{c_p}{D_{po}} \right) &= -\frac{c_p c_\Sigma}{RT} \nabla \mu_p + \frac{c_p c_s}{D_{ps}} u_s \\ -N_p \left(\frac{c_m}{D_{pm}} \right) + N_m \left(\frac{c_p}{D_{pm}} + \frac{c_o}{D_{mo}} + \frac{c_s}{D_{ms}} \right) - N_o \left(\frac{c_m}{D_{mo}} \right) &= -\frac{c_m c_\Sigma}{RT} \nabla \mu_m + \frac{c_m c_s}{D_{ms}} u_s \\ -N_p \left(\frac{c_o}{D_{po}} \right) - N_m \left(\frac{c_o}{D_{mo}} \right) + N_o \left(\frac{c_p}{D_{po}} + \frac{c_m}{D_{mo}} + \frac{c_s}{D_{so}} \right) &= -\frac{c_o c_\Sigma}{RT} \nabla \mu_o + \frac{c_o c_s}{D_{so}} u_s \end{aligned} \right\} \quad (\text{S15})$$

The ionic current is a combination of anionic and cationic fluxes, $I = F \sum_i z_i N_i$:

$$\therefore I/F = z_p N_p + z_m N_m \quad (\text{S16})$$

Substituting for N_m in terms of I and N_p from (S16) in (S15):

$$N_p \left(\frac{c_o}{D_{po}} + \frac{c_s}{D_{ps}} \right) - I/F z_m \left(\frac{c_p}{D_{pm}} \right) - N_o \left(\frac{c_p}{D_{po}} \right) = -\frac{c_p c_\Sigma}{RT} \nabla \mu_p + \frac{c_p c_s}{D_{ps}} u_s \quad (\text{S17a})$$

$$-\frac{N_p z_p}{z_m} \left(\frac{c_o}{D_{mo}} + \frac{c_s}{D_{ms}} \right) - N_o \left(\frac{c_m}{D_{mo}} \right) + I/F z_m \left(\frac{c_p}{D_{pm}} + \frac{c_o}{D_{mo}} + \frac{c_s}{D_{ms}} \right) = -\frac{c_m c_\Sigma}{RT} \nabla \mu_m + \frac{c_m c_s}{D_{ms}} u_s \quad (\text{S17b})$$

$$N_p c_o \left(\frac{z_p D_{po} - z_m D_{mo}}{z_m D_{po} D_{mo}} \right) + N_o \left(\frac{c_p}{D_{po}} + \frac{c_m}{D_{mo}} + \frac{c_s}{D_{so}} \right) - I/F z_m \left(\frac{c_o}{D_{mo}} \right) = -\frac{c_o c_\Sigma}{RT} \nabla \mu_o + \frac{c_o c_s}{D_{so}} u_s \quad (\text{S17c})$$

Note that the (electro-) chemical potential gradients cause the fluxes, and to further use them in species balance, the fluxes are to be expressed in terms of the driving forces (*i.e.*, the gradients). However, the mathematical nature of the Stefan – Maxwell relations provides a linear combination of species fluxes against each of the driving forces (Eq. (S17)). To obtain explicit species flux expressions, equations presented in (S17) need to be reshuffled. Mathematically, it is equivalent to a matrix inversion to express three species fluxes as a combination of three gradients¹. The first two expressions can be linearly added to eliminate solvent flow (local charge neutrality Eq. (S5) is used to simplification):

$$\begin{aligned} I/F \left(c_m \frac{D_{ps}}{D_{pm}} + c_p \frac{D_{ms}}{D_{pm}} + c_o \frac{D_{ms}}{D_{mo}} + c_s \right) &= -z_p \frac{c_p c_\Sigma}{RT} (D_{ps} \nabla \mu_p - D_{ms} \nabla \mu_m) \\ &- N_p z_p c_o \left(\frac{D_{ps}}{D_{po}} - \frac{D_{ms}}{D_{mo}} \right) + N_o z_p c_p \left(\frac{D_{ps}}{D_{po}} - \frac{D_{ms}}{D_{mo}} \right) \end{aligned} \quad (\text{S18})$$

Similarly, using the first two expressions in (S17) to eliminate the oxygen flux:

$$\begin{aligned} N_p z_p c_s \left(\frac{D_{po}}{D_{ps}} - \frac{D_{mo}}{D_{ms}} \right) &= -z_p \frac{c_p c_\Sigma}{RT} (D_{po} \nabla \mu_p - D_{mo} \nabla \mu_m) + z_p c_p \left(\frac{D_{po}}{D_{ps}} - \frac{D_{mo}}{D_{ms}} \right) c_s u_s \\ &- I/F \left(c_m \frac{D_{po}}{D_{pm}} + c_p \frac{D_{mo}}{D_{pm}} + c_o + c_s \frac{D_{mo}}{D_{ms}} \right) \end{aligned} \quad (\text{S19})$$

To aid the simplification, recurring groups of properties are defined as shown in Table S1. Using these mixed variables, the last expression in (S17) can be rewritten as:

$$N_o \left(\frac{v c}{D_o} + \frac{c_s}{D_{so}} \right) = -\frac{c_o c_\Sigma}{RT} \nabla \mu_o + \frac{c_o c_s}{D_{so}} u_s + N_p \left(\frac{v c_o}{v_p D_o} \right) + I/F z_m \left(\frac{c_o}{D_{mo}} \right) \quad (\text{S20})$$

Alternatively, summing the three linear equations in (S17):

$$N_o \left(\frac{c_s}{D_{so}} \right) = -\frac{c_o c_\Sigma}{RT} \nabla \mu_o + \left(\frac{v c}{D_s} + \frac{c_o}{D_{so}} \right) c_s u_s - N_p \left(\frac{v c_s}{v_p D_s} \right) - I/F z_m \left(\frac{c_s}{D_{ms}} \right) - \frac{c c_\Sigma}{RT} \nabla \mu \quad (\text{S21})$$

Eliminating cation flux, N_p , from Eq. (S20) and (S21) via linear operation:

$$N_o \left(\frac{\nu c}{D_o} + \frac{c_s}{D_{so}} \left(1 + \frac{c_o}{c_s} \cdot \frac{D_s}{D_o} \right) \right) = - \frac{c_o c_\Sigma}{RT} \left(1 + \frac{c_o}{c_s} \cdot \frac{D_s}{D_o} \right) \nabla \mu_o$$

$$+ \left(\frac{c_o}{D_{so}} \left(1 + \frac{c_o}{c_s} \cdot \frac{D_s}{D_o} \right) + \frac{\nu c c_o}{c_s D_o} \right) c_s u_s + I / F z_m \left(\frac{c_o}{D_{mo}} - \frac{c_o D_s}{D_{ms} D_o} \right) - \frac{c c_\Sigma}{RT} \cdot \frac{c_o D_s}{c_s D_o} \nabla \mu$$

Table S1. Mixed variables appearing in electrolyte transport description.

Mixed variable	Expression	Associated relations
t_p^s , cationic elemental transference number in solvent frame	$t_p^s = \frac{z_p D_{ps}}{z_p D_{ps} - z_m D_{ms}} = \frac{\nu_m D_{ps}}{\nu_m D_{ps} + \nu_p D_{ms}}$	$t_p^s + t_m^s = 1$ $D_{ps} = \frac{\nu_p D_s}{\nu t_m^s}$
D_s , salt diffusivity in solvent frame	$D_s = \frac{(z_p - z_m) D_{ps} D_{ms}}{z_p D_{ps} - z_m D_{ms}} = \frac{\nu D_{ps} D_{ms}}{\nu_m D_{ps} + \nu_p D_{ms}}$	$D_{ms} = \frac{\nu_m D_s}{\nu t_p^s}$
t_p^o , cationic elemental transference number in oxygen frame	$t_p^o = \frac{z_p D_{po}}{z_p D_{po} - z_m D_{mo}} = \frac{\nu_m D_{po}}{\nu_m D_{po} + \nu_p D_{mo}}$	$t_p^o + t_m^o = 1$ $D_{po} = \frac{\nu_p D_o}{\nu t_m^o}$
D_o , salt diffusivity in oxygen frame	$D_o = \frac{(z_p - z_m) D_{po} D_{mo}}{z_p D_{po} - z_m D_{mo}} = \frac{\nu D_{po} D_{mo}}{\nu_m D_{po} + \nu_p D_{mo}}$	$D_{mo} = \frac{\nu_m D_o}{\nu t_p^o}$
	$\frac{c_s}{D_{ps}} - \frac{z_p}{z_m} \frac{c_s}{D_{ms}} = c_s \left(\frac{1}{\nu_p D_s / \nu t_m^s} + \frac{\nu_m}{\nu_p} \cdot \frac{1}{\nu_m D_s / \nu t_p^s} \right) = \frac{\nu c_s}{\nu_p D_s}$	
	$\frac{z_p D_{po} - z_m D_{mo}}{z_m D_{po} D_{mo}} = \frac{(z_p - z_m)}{z_m} \left\{ \frac{z_p D_{po} - z_m D_{mo}}{(z_p - z_m) D_{po} D_{mo}} \right\} = - \frac{\nu}{\nu_p D_o}$	
	$\frac{c_p}{D_{ps}} + \frac{c_m}{D_{ms}} = \frac{\nu_p c}{\left(\frac{\nu_p D_s}{\nu t_m^s} \right)} + \frac{\nu_m c}{\left(\frac{\nu_m D_s}{\nu t_p^s} \right)} = \frac{\nu c}{D_s}$	
	$\frac{c_p}{D_{po}} + \frac{c_m}{D_{mo}} = \frac{\nu_p c}{\left(\frac{\nu_p D_o}{\nu t_m^o} \right)} + \frac{\nu_m c}{\left(\frac{\nu_m D_o}{\nu t_p^o} \right)} = \frac{\nu c}{D_o}$	
γ , diffusability (relative ability of salt to diffuse in solvent as compared to oxygen)	$\gamma = 1 + \frac{c_o}{c_s} \cdot \frac{D_s}{D_o}$	

	$c_m \frac{D_{ps}}{D_{pm}} + c_p \frac{D_{ms}}{D_{pm}} = \frac{c}{D_{pm}} \left(v_m \cdot \frac{v_p D_s}{v t_m^s} + v_p \cdot \frac{v_m D_s}{v t_p^s} \right) = \frac{v_p v_m}{v} \cdot \frac{D_s}{D_{pm}} \cdot \frac{c}{t_p^s t_m^s}$
	$c_m \frac{D_{po}}{D_{pm}} + c_p \frac{D_{mo}}{D_{pm}} = \frac{c}{D_{pm}} \left(v_m \cdot \frac{v_p D_o}{v t_m^o} + v_p \cdot \frac{v_m D_o}{v t_p^o} \right) = \frac{v_p v_m}{v} \cdot \frac{D_o}{D_{pm}} \cdot \frac{c}{t_p^o t_m^o}$
	$D_{ps} \nabla \mu_p - D_{ms} \nabla \mu_m = \frac{D_s}{v} \left(\frac{v_p \nabla \mu_p}{t_m^s} - \frac{v_m \nabla \mu_m}{t_p^s} \right) = \frac{D_s}{v t_p^s} \left(\frac{v_p \nabla \mu_p}{t_m^s} - \nabla \mu \right)$
	$D_{po} \nabla \mu_p - D_{mo} \nabla \mu_m = \frac{D_o}{v} \left(\frac{v_p \nabla \mu_p}{t_m^o} - \frac{v_m \nabla \mu_m}{t_p^o} \right) = \frac{D_o}{v t_p^o} \left(\frac{v_p \nabla \mu_p}{t_m^o} - \nabla \mu \right)$
	$\frac{D_{ps}}{D_{po}} - \frac{D_{ms}}{D_{mo}} = \frac{D_s}{D_o} \left(\frac{t_m^o}{t_m^s} - \frac{t_p^o}{t_p^s} \right)$
	$\frac{D_{po}}{D_{ps}} - \frac{D_{mo}}{D_{ms}} = \frac{D_o}{D_s} \left(\frac{t_m^s}{t_m^o} - \frac{t_p^s}{t_p^o} \right)$

Or,

$$N_o \left(\frac{v c}{D_o} + \frac{c_s \gamma}{D_{so}} \right) = -\frac{c_o c_\Sigma}{RT} \nabla \mu_o - \frac{c c_\Sigma}{RT} (\gamma - 1) \nabla \mu$$

$$+ \frac{I}{F} \cdot \frac{v c_o}{v_m z_m D_o} (t_p^o - t_p^s) + \left(\frac{v c}{D_o} + \frac{c_s \gamma}{D_{so}} \right) c_o u_s$$
(S22)

Similarly, simplified equivalents of (S18) and (S19) are:

$$\frac{I}{F} \left(\frac{v_p v_m}{v} \cdot \frac{D_s}{D_{pm}} \cdot \frac{c}{t_p^s t_m^s} + c_o \frac{D_s}{D_o} \cdot \frac{t_p^o}{t_p^s} + c_s \right) = -z_p \frac{c_p c_\Sigma}{RT} \cdot \frac{D_s}{v t_p^s} \left(\frac{v_p \nabla \mu_p}{t_m^s} - \nabla \mu \right)$$

$$- z_p \frac{D_s}{D_o} \left(\frac{t_m^o}{t_m^s} - \frac{t_p^o}{t_p^s} \right) (c_o N_p - c_p N_o)$$
(S23)

$$N_p z_p c_s \frac{D_o}{D_s} \left(\frac{t_m^s}{t_m^o} - \frac{t_p^s}{t_p^o} \right) = -z_p \frac{c_p c_\Sigma}{RT} \cdot \frac{D_o}{v t_p^o} \left(\frac{v_p \nabla \mu_p}{t_m^o} - \nabla \mu \right) + z_p c_s \frac{D_o}{D_s} \left(\frac{t_m^s}{t_m^o} - \frac{t_p^s}{t_p^o} \right) c_p u_s$$

$$- \frac{I}{F} \left(\frac{v_p v_m}{v} \cdot \frac{D_o}{D_{pm}} \cdot \frac{c}{t_p^o t_m^o} + c_o + c_s \frac{D_o}{D_s} \cdot \frac{t_p^s}{t_p^o} \right)$$
(S24)

Equations (S22) through (S24) are a restatement of (S17). Substituting N_p and N_o expressions from (S24) and (S22) into ionic current relation (S23), it can be shown that the total ionic current is a combination of migration and diffusive contributions:

$$I = -\kappa \nabla \phi_e - \tilde{\kappa} \nabla \ln c - \tilde{\kappa}_o \nabla \ln c_o$$
(S25)

with the ionic conductivity, κ , and the two diffusional conductivities, $\tilde{\kappa}$ and $\tilde{\kappa}_o$, defined as:

$$\kappa = \frac{1}{\text{denom}} \left\{ \frac{F^2 \nu_p^2 z_p^2}{\nu} \cdot \frac{c c_\Sigma}{RT} \cdot \frac{D_s}{t_p^s (1-t_p^s)} \gamma \right\} \quad (\text{S26})$$

$$\frac{\tilde{\kappa}}{\kappa} = -\frac{\nu^2 RT}{F \nu_p z_p} \cdot \frac{t_p^s (1-t_p^s)}{\gamma} \left(1 + \frac{d \ln f}{d \ln c} \right) \left\{ \frac{1}{\nu t_p^s} \left(1 + \frac{c_o D_s}{c_s D_o} \cdot \frac{t_m^o}{t_m^s} \right) + \frac{(t_p^o - t_p^s) c (\gamma - 1)}{t_p^s (1-t_p^s) D_o \left(\frac{\nu c}{D_o} + \frac{c_s \gamma}{D_{so}} \right)} \right\} \quad (\text{S27})$$

$$\frac{\tilde{\kappa}_o}{\kappa} = -\frac{\nu RT}{F \nu_p z_p} \cdot \frac{c_o}{D_o} (t_p^o - t_p^s) \frac{1}{\left(\frac{\nu c}{D_o} + \frac{c_s \gamma}{D_{so}} \right)} \quad (\text{S28})$$

$$\begin{aligned} \text{denom} &= \frac{\nu_p \nu_m}{\nu} \cdot \frac{D_s}{D_{pm}} \cdot \frac{c \gamma}{t_p^s (1-t_p^s)} + c_s \left\{ 1 + \frac{c_o D_s}{c_s D_o} \cdot \frac{t_m^o}{t_m^s} \right\} \\ &+ \frac{c_o D_s}{D_o} \left\{ \frac{t_p^o}{t_p^s} + \frac{c_o D_s}{c_s D_o} \cdot \frac{t_p^o t_m^o}{t_p^s t_m^s} + \frac{\nu z_p c_p (t_p^o - t_p^s)^2}{\nu_m z_m D_o t_p^s t_m^s \left(\frac{\nu c}{D_o} + \frac{c_s \gamma}{D_{so}} \right)} \right\} \end{aligned} \quad (\text{S29})$$

Similarly, the molar fluxes of oxygen (Eq. (S22)) and the cation (Eq. (S24)) reduces to the expressions (the ionic current expression is rearranged to substitute for $\nabla \phi_e$ in the cation flux):

$$N_o = -\mathcal{D}_{oo} \nabla c_o - \mathcal{D}_{op} \nabla c + \mathcal{J}_o I / F + c_o u_s \quad (\text{S30})$$

$$N_p = -\nu_p \mathcal{D}_{pp} \nabla c - \mathcal{D}_{po} \nabla c_o + \mathcal{J}_p I / F z_p + \nu_p c u_s \quad (\text{S31})$$

with the composite transport properties – diffusivities, \mathcal{D} , and transference numbers, \mathcal{J} , defined as follows:

$$\mathcal{D}_{oo} = \frac{\gamma c_\Sigma}{\left(\frac{\nu c}{D_o} + \frac{c_s \gamma}{D_{so}} \right)} \quad (\text{S32})$$

$$\mathcal{D}_{op} = \frac{\nu (\gamma - 1) c_\Sigma}{\left(\frac{\nu c}{D_o} + \frac{c_s \gamma}{D_{so}} \right)} \left(1 + \frac{d \ln f}{d \ln c} \right) \quad (\text{S33})$$

$$\mathcal{J}_o = \frac{\frac{\nu}{\nu_m z_m} \cdot \frac{c_o}{D_o} (t_p^o - t_p^s)}{\left(\frac{\nu c}{D_o} + \frac{c_s \gamma}{D_{so}} \right)} \quad (\text{S34})$$

$$\mathcal{D}_{pp} = \frac{c_\Sigma}{c_s} D_s \left(1 + \frac{d \ln f}{d \ln c} \right) \left(\frac{\nu c}{D_o} + \frac{c_s}{D_{so}} \right) \left/ \left(\frac{\nu c}{D_o} + \frac{c_s \gamma}{D_{so}} \right) \right. \quad (\text{S35})$$

$$\mathcal{D}_{po} = \nu_p \frac{c c_\Sigma}{c_s} \cdot \frac{D_s}{D_o} \left/ \left(\frac{\nu c}{D_o} + \frac{c_s \gamma}{D_{so}} \right) \right. \quad (\text{S36})$$

$$\mathcal{J}_p = t_p^s - \left\{ (\gamma - 1) (t_p^s - t_p^o) \frac{c_s}{D_{so}} \left/ \left(\frac{\nu c}{D_o} + \frac{c_s \gamma}{D_{so}} \right) \right. \right\} \quad (\text{S37})$$

Partial Solubility Approximation:

Out of nine composite properties (ionic conductivity, two diffusional conductivities, four diffusivities, and two transference numbers), only seven are independent. In other words, for a complete characterization of a Li-air electrolyte, seven separate tests are required (in contrast to four for a Li-ion electrolyte⁶), which proves to be an overwhelming argument against a more accurate transport description.

Oxygen is a sparingly soluble species in organic electrolytes, limiting its dissolved concentration to mM^{7,8}. This fact can be leveraged to simplify the transport description in the limit of one solute with minimal solubility. In the limit of $c_o \rightarrow 0$ (i.e., $\gamma \rightarrow 1$), the expressions for the (composite) transport properties become:

$$\frac{1}{\kappa} \approx \frac{RT}{F^2 z_p^2 \nu_p^2 c_\Sigma} \left\{ \frac{\nu_p \nu_m}{D_{pm}} + \frac{\nu c_s t_p^s (1 - t_p^s)}{c D_s} \right\} \quad (\text{S38})$$

$$\frac{\tilde{\kappa}}{\kappa} = -\frac{\nu RT}{F} \cdot \frac{(1 - t_p^s)}{\nu_p z_p} \left(1 + \frac{d \ln f}{d \ln c} \right) \quad (\text{S39})$$

$$\frac{\tilde{\kappa}_o}{\kappa} \approx 0 \quad (\text{S40})$$

$$\mathcal{D}_{oo} \approx \frac{D_{so}}{\left(1 + \frac{\nu c D_{so}}{\gamma c_s D_o} \right)} = \frac{D_{so}}{\left(1 + \frac{\nu c D_{so}}{c_s D_o} \right)} \quad (\text{S41})$$

$$\mathcal{D}_{op} \approx 0 \quad (\text{S42})$$

$$\mathcal{J}_o \approx 0 \quad (\text{S43})$$

$$\mathcal{D}_{pp} \approx \frac{c_\Sigma}{c_s} D_s \left(1 + \frac{d \ln f}{d \ln c} \right) \quad (\text{S44})$$

$$\mathcal{D}_{po} \approx \frac{\nu_p c_\Sigma}{\nu c_s} D_s \left/ \left(1 + \frac{\gamma c_s D_o}{\nu c D_{so}} \right) \right. = \frac{\nu_p c_\Sigma}{\nu c_s} D_s \left/ \left(1 + \frac{c_s D_o}{\nu c D_{so}} \right) \right. \quad (\text{S45})$$

$$\mathcal{J}_p = t_p^s \quad (\text{S46})$$

where the expressions for κ , $\tilde{\kappa}$, \mathcal{D}_{pp} and \mathcal{J}_p reduce to those for a typical electrolyte². The relations for \mathcal{D}_{oo} and \mathcal{D}_{po} deserve a detailed discussion. In the limit $c_o \rightarrow 0$, total concentration $c_\Sigma = c_s + c_p + c_m + c_o$ simplifies to $c_\Sigma \rightarrow c_s + \nu c$. For typical electrolytes, solvent concentration is an order of magnitude higher, *e.g.*, for a 1M *LiTFSI* in DME, $\nu = 2$, $c = 1\text{M}$ and $c_s \approx 9.6\text{M}$ (solvent properties⁸ $\rho = 0.86370\text{ g/cc}$ and $M = 90\text{ g/mol}$). Hence, $1 + \nu c / c_s \approx 1$. However, $\nu c D_{so} / \gamma c_s D_o$ does not vanish in the limit of limited oxygen solubility. When oxygen solubility is measured (or computed) in the pure solvent³, it provides an estimate for the elemental diffusivity D_{so} , while in the presence of other solutes (here dissociated ions), the effective diffusivity is less (the denominator in (S41) is always greater than one). The elemental diffusivity D_{so} is often an order of magnitude higher than salt diffusivity (in electrolyte frame) D_s . Assuming equivalent solvation structure, it can be argued that the salt diffusivity D_o in oxygen frame exhibits a similar qualitative and quantitative dependence, and in turn, the magnitude of $\nu c D_{so} / \gamma c_s D_o$ is not necessarily negligible in comparison to unity (Eq. (S41) and (S45)). The difference in solvation structure for oxygen diffusion with and without the lithium salt in the electrolyte is presented in Fig S1. The impediment caused due to the presence of the additional solute entities is phenomenologically equivalent to reduced diffusion in porous electrodes. In the same spirit, the stochastic structure of additional solutes can be characterized in terms of a ‘*solute tortuosity*’ as Eq. (S47).

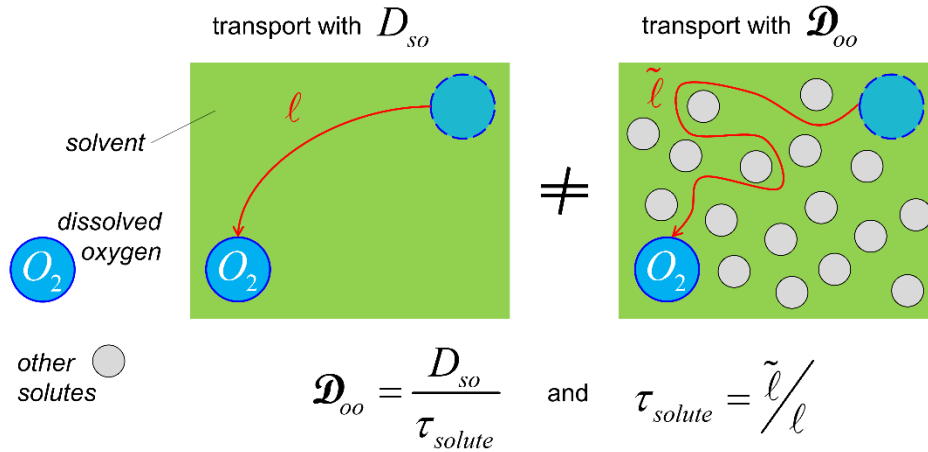


Fig S1. Diffusion characteristics of oxygen change in the presence of additional solutes (here ions).

$$\tau_{solute} = 1 + \frac{\nu c D_{so}}{c_s D_o} \quad (\text{S47})$$

In the limit of no salt concentration, $\tau_{solute} \rightarrow 1$ ($\tau_{solute} \geq 1$).

Given the interaction among the ions and (dissolved) oxygen molecules, the cross-diffusivity in cation transport (Eq. (S45)) is affected by local solute structure (Fig. S1). The cross-diffusion coefficient, \mathcal{D}_{po} can be expressed in terms of solute tortuosity, τ_{solute} as:

$$\mathcal{D}_{po} = \frac{v_p}{v} \frac{c_\Sigma}{c_s} D_s \left(\frac{\tau_{solute} - 1}{\tau_{solute}} \right) = \frac{v_p}{v} \frac{c_\Sigma}{c_s} D_s \left(1 - \frac{1}{\tau_{solute}} \right) \quad (\text{S48})$$

The cross-diffusivity, \mathcal{D}_{po} vanishes as salt concentration reduces since as solute number density decreases the inter-solute distances become larger than the interaction lengths for short-range potentials. Typical salt concentrations are high enough to lead to such cross-interactions. Such concentration dependence in solute tortuosity impedes oxygen transport, *i.e.*, locally causing larger gradients in oxygen concentration which coincides with high cross diffusion for cation flux. The concentration profiles for cation (here Li^+) and dissolved oxygen are negatively correlated in the porous electrode for Li-oxygen electrochemistry (Fig S2), which in the extreme conditions cause cation flux against its concentration gradient (similar to ‘up-hill diffusion’ in alloys⁹).

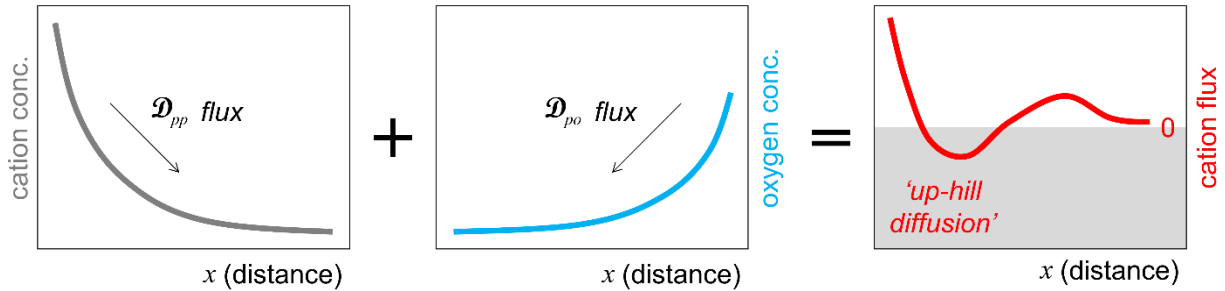


Fig S2. Multi-species complexations in transport interactions.

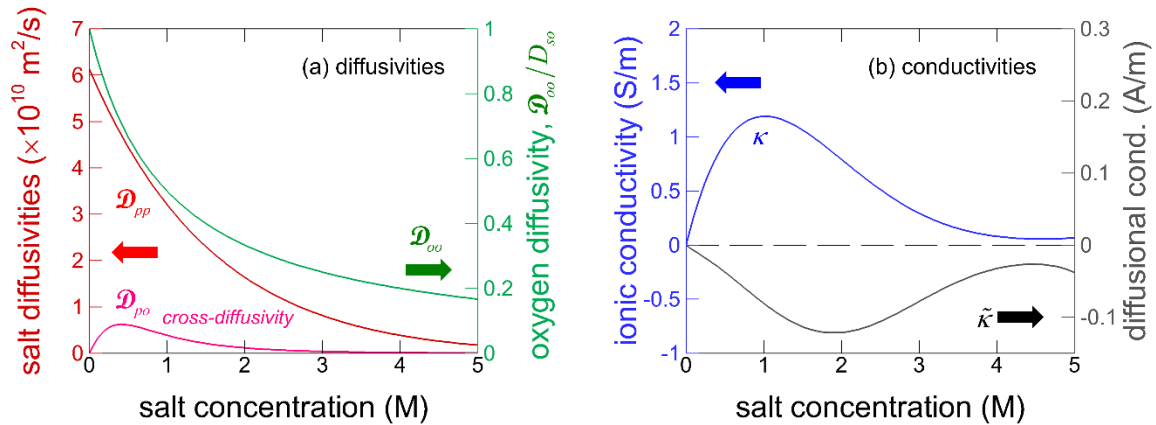


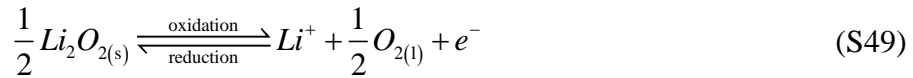
Fig S3. Transport properties for a Li-oxygen electrolyte.

The ‘concentrated solution theory’ and its subsequent simplification discussed here (referred to as ‘partial solubility approximation’) are disparate from the ‘dilute solution theory’ where mutual

interactions are not accounted for. The usefulness of such simplification lies in reducing the number of experimental tests required for a thorough characterization from seven to five. The cross diffusivity \mathcal{D}_{po} can be estimated from a combination of \mathcal{D}_{oo} , \mathcal{D}_{pp} and $\tilde{\kappa}/\kappa$. Based on the electrolyte transport properties of a Li-ion electrolyte and accounting for electrolyte description developed here, the complete set of transport properties can be obtained for an equivalent Li-oxygen electrolyte (Fig S3).

S2. Reaction Kinetics with an Insulating Insoluble Reactant

The primary reaction responsible for (electrochemical) energy storage in Li-oxygen cathode (with organic electrolyte) is lithium peroxide, Li_2O_2 , formation. It is fundamentally an electrodeposition reaction that deposits solid lithium peroxide. However, it differs from traditionally known electrodeposition sequences, *e.g.*, lithium plating¹⁰, in that the depositing phase – Li_2O_2 – is electronically insulating. Electronic conductivity of the solid in contact with the electrolyte is essential to providing electrons to sustain the reduction reaction. Since Li_2O_2 is electronically insulating, reduction sites change in time (once the local Li_2O_2 thickness is greater than the ‘*tunneling length*’, the nucleation site becomes unavailable for further reduction). Every phase-change reaction exhibits stochastic spatial variations at microscopic length-scales given the distribution of nucleation sites^{11, 12}. Fig S5(a) highlights such a distributed nature of the reaction (S49). An appropriate kinetic description of such a reaction scheme is absent from the literature.



For the reaction (S49), an equilibrium condition is related to (electro-) chemical potentials of participating species²:

$$\frac{1}{2} \mu_{Li_2O_{2(s)}} = \mu_{Li^+} + \frac{1}{2} \mu_{O_{2(l)}} + \mu_{e^-} \quad (S50)$$

Correspondingly, the driving force for the reaction, *i.e.*, overpotential is defined as (per unit electron transfer):

$$\eta = \frac{1}{F} \left\{ \frac{1}{2} \mu_{Li_2O_{2(s)}} - \left(\mu_{Li^+} + \frac{1}{2} \mu_{O_{2(l)}} + \mu_{e^-} \right) \right\} \quad (S51)$$

Even if electrolyte contact exists along the entire electrode-electrolyte interface, only a part is available for electrolyte phase species to react. Let this surface reactivity be denoted as θ_e . The expressions for (electro-) chemical potentials of the electrolyte phase species subsequently become:

$$\mu_{Li^+} = \mu_{Li^+}^0 + F\phi_e + RT \log(\theta_e c_p / c_p^{\text{ref}}) \quad (S52)$$

$$\mu_{O_{2(l)}} = \mu_{O_{2(l)}}^0 + RT \log(\theta_e c_o / c_o^{\text{ref}}) \quad (S53)$$

Note that θ_e is surface activity, and in the bulk of the electrolyte, the expressions (S6) and (S7) are still applicable. Similarly, let the surface activity of Li_2O_2 be θ_s , and equivalently the chemical potential responsible for the equilibrium (S51) is:

$$\mu_{Li_2O_{2(s)}} = \mu_{Li_2O_{2(s)}}^0 + RT \log(\theta_s) \quad (S54)$$

where $\mu_{Li_2O_{2(s)}}^0$ is chemical potential in the limit of complete surface coverage (*i.e.*, $\theta_s \rightarrow 1$).

Substituting Eq. (S52) to (S54) in (S51):

$$\eta = \frac{1}{F} \left\{ \begin{array}{l} \frac{1}{2} \left(\mu_{Li_2O_{2(s)}}^0 + RT \log \theta_s \right) \\ - \left(\mu_{Li^+}^0 + F\phi_e + RT \log(\theta_e c_p) \right) - \frac{1}{2} \left(\mu_{O_{2(l)}}^0 + RT \log(\theta_e c_o) \right) - (-F\phi_s) \end{array} \right\} = \phi_s - \phi_e - U \quad (S55)$$

with the open circuit potential (OCP) expressions:

$$U = U^0 + \frac{RT}{F} \log \left(\left(\frac{\theta_e c_p}{c_p^{\text{ref}}} \right) \left(\frac{\theta_e c_o}{c_o^{\text{ref}}} \right)^{1/2} / \sqrt{\theta_s} \right) \quad (S56)$$

$$U^0 = \left(\mu_{Li^+}^0 + \frac{1}{2} \mu_{O_{2(l)}}^0 - \frac{1}{2} \mu_{Li_2O_{2(s)}}^0 \right) \quad (S57)$$

U^0 is OCP at reference concentrations and temperature. Equation (S56) is the extended Nernst equation for unequal surface activities (Fig S4).

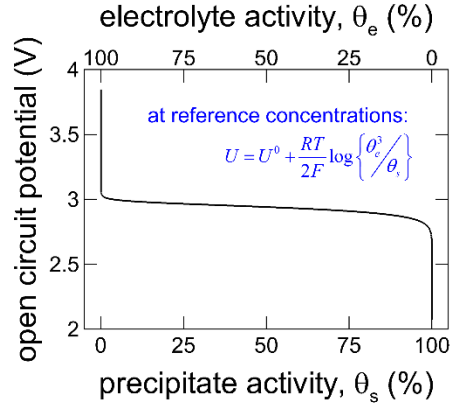


Fig S4. At reference concentrations, the open circuit potential varies with the activity of the precipitate phase, and equivalently the activity of the electrolyte phase.

The energy landscape corresponding to reaction (S49) is shown in Fig S5(b), where Δg^f and Δg^b are driving forces for the forward and backward reaction halves (*i.e.*, oxidation and reduction, respectively). Since the potential energy of Li_2O_2 (*i.e.*, chemical potential) is smaller than the electrolyte phase species, the formation of Li_2O_2 is thermodynamically spontaneous and in turn,

represent the energy producing (discharge) half. Based on the law of mass action¹³, corresponding molar rates can be expressed as:

$$r^f = k^f \sqrt{\theta_s} = \left[k^{f0} \exp(-\Delta g^f / RT) \right] \sqrt{\theta_s} \quad (\text{S58})$$

$$r^b = k^b (\theta_e c_p) \sqrt{\theta_e c_o} = \left[k^{b0} \exp(-\Delta g^b / RT) \right] (\theta_e c_p) \sqrt{\theta_e c_o} \quad (\text{S59})$$

where the rate constants are related to activation energies via Arrhenius expressions¹³. The (balanced) reaction (S49) is written in as a single electron reaction, and equivalently the reaction current (units of A/m²) is:

$$\frac{i}{F} = r^f - r^b = \left[k^{f0} \exp(-\Delta g^f / RT) \right] \sqrt{\theta_s} - \left[k^{b0} \exp(-\Delta g^b / RT) \right] (\theta_e c_p) \sqrt{\theta_e c_o} \quad (\text{S60})$$

At equilibrium the energy barriers for the reaction halves are identical and the reactant concentrations approach their reference values, *i.e.*, the following equalities hold:

$$\Delta g_{eq}^f = \Delta g_{eq}^b \quad (\text{S61})$$

$$k^{f0} = k^{b0} c_p^{\text{ref}} \sqrt{c_o^{\text{ref}}} = k^0 \quad (\text{S62})$$

$$U = U^0 \quad (\text{S63})$$

Substituting relations (S61) and (S62) in current density (S60):

$$i = Fk^0 \exp(-\Delta g_{eq}^f / RT) \left\{ \sqrt{\theta_s} \exp\left(-\frac{(\Delta g^f - \Delta g_{eq}^f)}{RT}\right) - \left(\frac{\theta_e c_p}{c_p^{\text{ref}}}\right) \sqrt{\frac{\theta_e c_o}{c_o^{\text{ref}}}} \exp\left(-\frac{(\Delta g^b - \Delta g_{eq}^b)}{RT}\right) \right\} \quad (\text{S64})$$

To drive the reaction in either direction, the potential difference is varied (*e.g.*, cyclic voltammetry systematically changes solid phase potential, ϕ_s , to characterize electrochemical reactions²). The applied potential difference affects both the activation energies. Let the partition of this influence be α and $(1-\alpha)$, respectively to anodic (forward) and cathodic (backward) halves (Fig S5(b)). Thence, the free energy differences appearing in Eq. (S64) can be expressed as:

$$\Delta g^f - \Delta g_{eq}^f = -\alpha F (\phi_s - \phi_e - U^0) \quad (\text{S65})$$

$$\Delta g^b - \Delta g_{eq}^b = (1-\alpha) F (\phi_s - \phi_e - U^0) \quad (\text{S66})$$

and the reaction current density expression (S64) becomes:

$$i = Fk^0 \exp(-\Delta g_{eq}^f / RT) \left\{ \sqrt{\theta_s} e^{\frac{\alpha F (\phi_s - \phi_e - U^0)}{RT}} - \left(\frac{\theta_e c_p}{c_p^{\text{ref}}}\right) \sqrt{\frac{\theta_e c_o}{c_o^{\text{ref}}}} e^{\frac{-(1-\alpha) F (\phi_s - \phi_e - U^0)}{RT}} \right\} \quad (\text{S67})$$

Standard OCP appearing in (S67) can be replaced in terms of its concentration dependent counterpart using Eq. (S56), to yield an alternate form of reaction kinetics (S67):

$$i = Fk^0 \exp(-\Delta g_{eq}^f / RT) \left[\left(\frac{\theta_e c_p}{c_p^{\text{ref}}}\right) \sqrt{\frac{\theta_e c_o}{c_o^{\text{ref}}}} \right]^\alpha \left[\sqrt{\theta_s} \right]^{(1-\alpha)} \left\{ e^{\frac{\alpha F (\phi_s - \phi_e - U)}{RT}} - e^{\frac{-(1-\alpha) F (\phi_s - \phi_e - U)}{RT}} \right\} \quad (\text{S68})$$

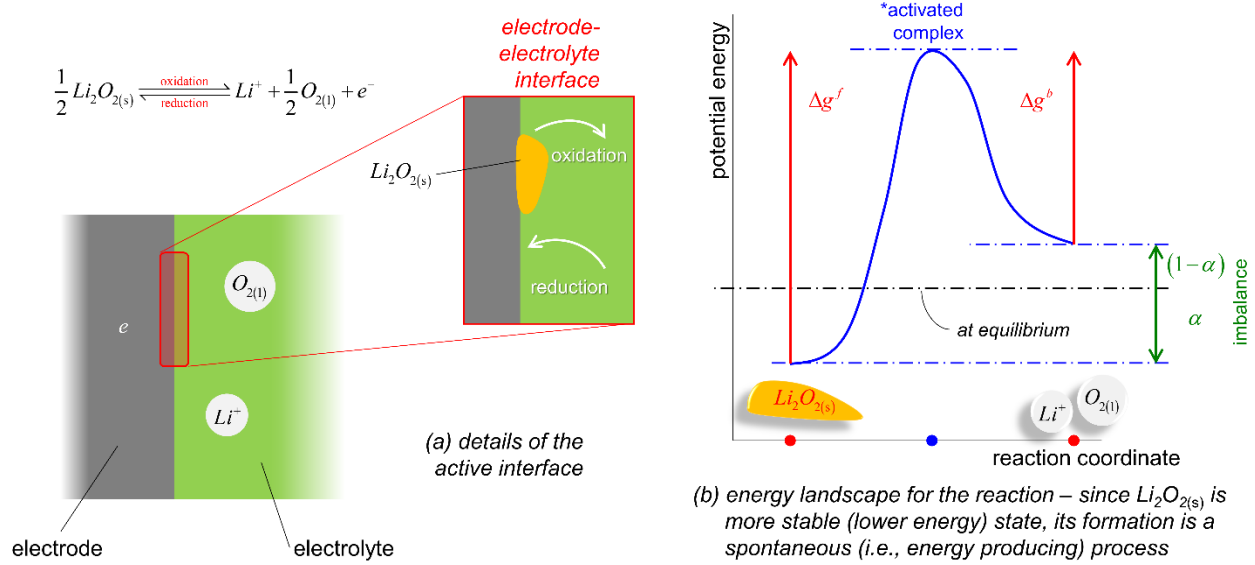


Fig S5. Electronic conductivity of the precipitate phase plays a crucial role in the corresponding reaction scheme.

Or, expressed more concisely,

$$i = i^0 \left\{ e^{\frac{\alpha F \eta}{RT}} - e^{-\frac{(1-\alpha) F \eta}{RT}} \right\} \quad (S69)$$

where the overpotential, $\eta = \phi_s - \phi_e - U$, varies with local concentration (Fig S4) and the exchange current density, i^0 , has the form:

$$i^0 = Fk^0 \exp(-\Delta g_{eq}^f / RT) \left[\left(\frac{\theta_e c_p}{c_p^{\text{ref}}} \right) \sqrt{\frac{\theta_e c_o}{c_o^{\text{ref}}}} \right]^\alpha \left[\sqrt{\theta_s} \right]^{(1-\alpha)} \quad (S70)$$

The expressions (S67) and (S68) are alternate forms of the Butler – Volmer kinetics with insulating precipitates. These expressions are directly valid for planar electrodes. The two different expressions offer analytical advantages based on the desired application. For example, interpretation of cyclic voltammetry¹⁴ is more straight forward with standard OCP form (Eq. (S67)), while impedance spectroscopy¹⁵ data is more amenable to a state of charge dependent OCP (Eq. (S68)). For a porous electrode, appropriate volumetric current density (A/m^3) has the expression:

$$j = a^0 i \quad (S71)$$

where a^0 is the total solid – electrolyte interfacial area (i.e., BET area). Total area, a^0 , is not necessarily equal to the active area for each of the reactions. The incorporation of surface activities provides a consistent representation for the reaction at intermediate length-scales equivalent to pore dimensions. At smaller length-scales, one has to explicitly account for each of the reaction halves and their interfacial distribution¹⁶⁻²⁰.

S3. Abstracting Porous Electrode Evolution upon Precipitation

The porous electrodes for Li-oxygen are unique in that they exhibit considerable geometrical evolution during each operation, thus making a reliable quantification of the microstructure growth essential to comprehending the associated electrochemical complexations. Here electrode structures composed of fibers are studied. Authors have previously reported the evolutionary response of other geometrical arrangements²¹⁻²³. As shown in Fig S6, the pristine structure is specified in terms of fiber dimension (here diameter, D^0) and pristine porosity, ε^0 . Each of the pristine structures is evolved by growing (mesoscopic) precipitates with varying morphology, ω , and amounts, ε_p (m^3 of precipitate/ m^3 of electrode microstructure). Fig S6 shows a representative evolved structure. Such representative structures are large enough to contain sufficient material distribution to behave as a porous medium, *i.e.*, are of RVE (representative volume element) dimensions²⁴. The pristine structures are generated in GeoDict^{25, 26}, while coarse-grained precipitate growth is described through an interfacial energy based approach^{21, 22}.

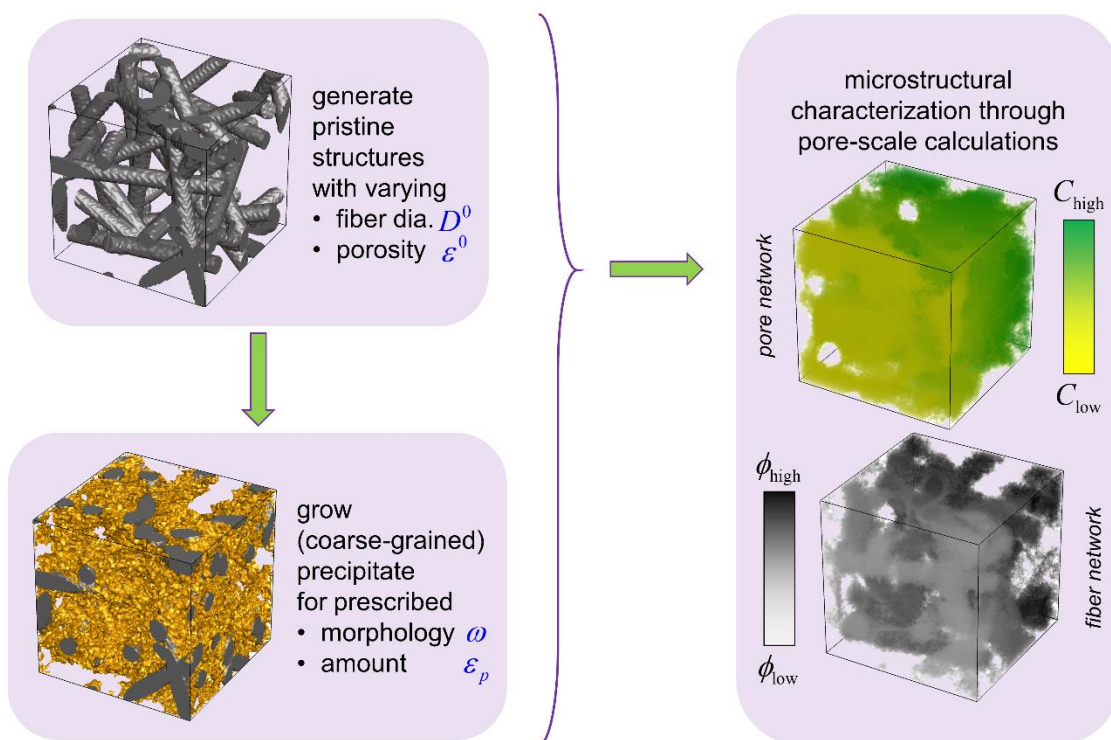


Fig S6. An outline of electrode microstructure generation and subsequent characterization.

Each of these microstructural representations are subsequently characterized to estimate effective properties (Table S2) relevant to species transport through the pore network (namely tortuosity), electron conduction through the fiber network (*i.e.*, electronic conductivity), and kinetics at the solid – pore interface (interfacial area directly correlates to surface activities that affect electrochemical reactions). Various two-phase interfaces are measured as per the modified Minkowski measure^{21, 22}, while tortuosity and effective electronic conductivities are estimated

through pore-scale solutions of species balance and potential balance^{21, 22}, respectively. Fig S6 also demonstrates representative solutions to these equations. Once the sufficient number of representative structures are characterized, the resultant dataset is analyzed to extract functional relations that quantitatively describe the microstructural evolution upon precipitation. Table S2 presents such correlations for the pristine fibrous structure.

Table S2. Microstructural evolution is quantified in terms of effective property variation upon precipitation

Property	Expression
Carbon – electrolyte interfacial area	$a_{01} = \frac{1}{D^0} \left(-0.038 + 4.043(1 - \varepsilon^0) - 2.316(1 - \varepsilon^0)^2 \right) \left\{ 1 - \left(\frac{\varepsilon_p}{0.452\omega^{2.751}} \right)^{1.1} \right\}$
Carbon – precipitate interfacial area	$a_{12} = \frac{\varepsilon_p}{D^0} \left(0.066 + 12.909(1 - \varepsilon^0) - 10.002(1 - \varepsilon^0)^2 \right) (2.485 - 4.235\varepsilon_p - 0.171\omega)$
Precipitate – electrolyte contact area	$a_{20} = \frac{\varepsilon_p}{D^0} \left(1.279 + 3.776(1 - (\varepsilon^0 - \varepsilon_p)) - 0.780(1 - (\varepsilon^0 - \varepsilon_p))^2 \right) (5.079 - 10.498\varepsilon_p + 0.288\omega)$
Pristine carbon surface area	$a_{1(0+2)} = \frac{\varepsilon_p}{D^0} \left(-0.005 + 4.031(1 - \varepsilon^0) - 2.632(1 - \varepsilon^0)^2 \right)$
Pore network tortuosity	$\tau = (0.967 + \varepsilon_p (1.209 - 5.730\varepsilon - 0.266\omega)) (\varepsilon^0 - \varepsilon_p)^{-(0.932 - \varepsilon_p (0.376 - 5.525\varepsilon - 0.607\omega))}$
Fiber network conductivity	$\sigma/\sigma^0 = 0.680(1 - \varepsilon^0)^{1.532}$

S4. Electrochemical Description of a Porous Evolving Electrode

The electrochemical response of a Li-oxygen porous electrode is a joint outcome of coupled interactions as summarized in Fig S7. Previous studies in the literature do not recognize such mesoscopic coupling and make unjustified assumptions, *e.g.*, resistive but not insulating Li_2O_2 ²⁷⁻²⁹, simpleton microstructural representation^{20, 30-33}, no inter-species interactions during transport³⁴⁻³⁶ and ad-hoc description of interfacial kinetics and subsequent growth^{37, 38}. To ameliorate such difficulties, here the mesoscopic interactions are coherently treated through non-equilibrium thermodynamics and pore-scale microstructural analysis. Mathematically, the following expressions govern the electrochemical evolution:

Cation (Li^+) transport in electrolyte:

$$\frac{\partial(\varepsilon c)}{\partial t} = \nabla \cdot \left(\mathcal{D}_{pp} \frac{\varepsilon}{\tau} \nabla c \right) + \nabla \cdot \left(\mathcal{D}_{po} \frac{\varepsilon}{\tau} \nabla c_o \right) + (1 - \mathcal{J}_p) j/F \quad (S72)$$

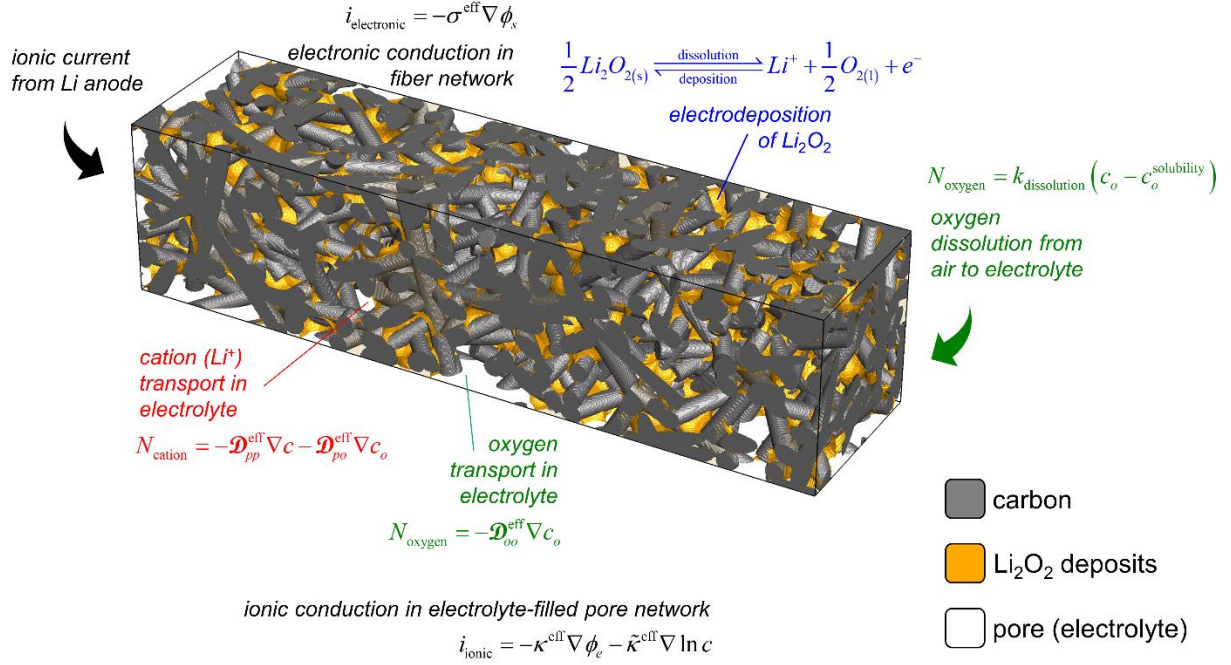


Fig S7. A graphical representation of various physicochemical interactions taking place in a porous electrode for Li-oxygen electrochemistry.

Oxygen (O_2) transport in electrolyte:

$$\frac{\partial(\varepsilon c_o)}{\partial t} = \nabla \cdot \left(\mathcal{D}_{oo} \frac{\varepsilon}{\tau} \nabla c_o \right) + j/2F \quad (\text{S73})$$

Ionic current in the electrolyte:

$$\nabla \cdot \left(\kappa \frac{\varepsilon}{\tau} \nabla \phi_e \right) + \nabla \cdot \left(\tilde{\kappa} \frac{\varepsilon}{\tau} \nabla \ln c \right) + j = 0 \quad (\text{S74})$$

Electronic current in the substrate network:

$$\sigma^{\text{eff}} \nabla^2 \phi_s = j \quad (\text{S75})$$

Lithium peroxide formation:

$$\frac{\partial \varepsilon_p}{\partial t} = -\frac{V_p j}{2F} \quad (\text{S76})$$

Porosity evolution:

$$\frac{\partial(\varepsilon + \varepsilon_p)}{\partial t} = 0 \quad (\text{S77})$$

where the reaction kinetics follows the expression (S64), and microstructural evolution follows the relations presented in Table S2. Note that the surface activities appearing in the kinetic description are intrinsically defined by respective interfacial area evolutions. Appropriate boundary and interface conditions are as follows (in the same sequence as equations (S72) to (S75)):

anode – separator boundary	separator – cathode interface	cathode – current collector boundary	
$-\mathcal{D}_{pp} \frac{\varepsilon}{\tau} \frac{\partial c}{\partial x} = (1 - \mathcal{J}_p) \frac{I_{\text{app}}}{F}$	<i>flux continuity</i>	$-\mathcal{D}_{pp} \frac{\varepsilon}{\tau} \frac{\partial c}{\partial x} = 0$	(S78)
$-\mathcal{D}_{oo} \frac{\varepsilon}{\tau} \frac{\partial c_o}{\partial x} = 0$	<i>flux continuity</i>	$-\mathcal{D}_{oo} \frac{\partial c_o}{\partial x} = k_{\text{dissolution}} (c_o - c_o^{\text{solubility}})$	(S79)
$-\kappa \frac{\varepsilon}{\tau} \frac{\partial \phi_e}{\partial x} - \tilde{\kappa} \frac{\varepsilon}{\tau} \frac{\partial \ln c}{\partial x} = I_{\text{app}}$	<i>flux continuity</i>	$\phi_e = 0$	(S80)
–	$-\sigma^{\text{eff}} \frac{\partial \phi_s}{\partial x} = 0$	$-\sigma^{\text{eff}} \frac{\partial \phi_s}{\partial x} = I_{\text{app}}$	(S81)

At the anode – separator interface, the oxygen flux vanishes, *i.e.*, $N_o = -\mathcal{D}_{oo} \frac{\varepsilon}{\tau} \frac{\partial c_o}{\partial x} = 0 \Rightarrow \frac{\partial c_o}{\partial x} = 0$

. Substituting this in the cation flux relation,

$$N_p = -\mathcal{D}_{pp} \frac{\varepsilon}{\tau} \frac{\partial c}{\partial x} - \mathcal{D}_{po} \frac{\varepsilon}{\tau} \frac{\partial c_o}{\partial x} + \mathcal{J}_p \frac{I_{\text{app}}}{F} = \frac{I_{\text{app}}}{F} \Rightarrow -\mathcal{D}_{pp} \frac{\varepsilon}{\tau} \frac{\partial c}{\partial x} = (1 - \mathcal{J}_p) \frac{I_{\text{app}}}{F},$$

since the ionic current at the anode – separator interface is purely due to cation generation. The solution algorithm for the evolving porous electrode (with time-varying microstructural properties) has been reported in the authors' earlier work²¹. Table S3 reports miscellaneous information regarding properties and operating conditions.

Table S3. Property values used in the electrochemical description

Property	Description	Remarks
a	Interfacial area (m^2/m^3)	Table S2
c	Salt concentration (initial $1000.0 \text{ mol}/\text{m}^3$)	
c_o	Oxygen concentration (initial $9.57 \text{ mol}/\text{m}^3$)	
$c_o^{\text{solubility}}$	Oxygen solubility in DME ($9.57 \text{ mol}/\text{m}^3$)	8
D_{so}	Oxygen diffusivity in the solvent ($5 \cdot 10^{-9} \text{ m}^2/\text{s}$)	7
D^0	Fiber diameter in pristine carbon structure (115 nm)	39
\mathcal{D}	Composite diffusivities	Fig S3
F	Faraday's constant (96 487 C/mol)	
I_{app}	Applied current (A/m^2 of electrode cross-section)	
I_d	Deposition current (A/m^2 of solid – electrolyte interface)	
i^0	Exchange current density ($10^{-5} \text{ A}/\text{m}^2$)	$i^0 = Fk^0 \exp(-\Delta g_{eq}^f / RT)$
$k_{\text{dissolution}}$	Dissolution rate constant ($10^{-4} \text{ m}/\text{s}$)	
L	Thickness (650 μm separator; 250 μm cathode)	39
R	Universal gas constant (8.314 J/mol·K)	
T	Operating temperature (25°C = 298.15 K)	
\mathcal{J}_p	Transference number (0.363)	6

V_p	Partial molar volume of Li_2O_2 ($2.1495 \cdot 10^{-5} \text{ m}^3/\text{mol}$)	
V_{cut}	Discharge cutoff voltage (1.5 V)	
<i>Greek symbols:</i>		
ε	Porosity (55% separator and 80% pristine cathode)	39
θ	Interfacial activity (between 0 and 1)	6
κ	Ionic conductivity	6
$\tilde{\kappa}$	Diffusional conductivity	6
τ	Tortuosity	Table S2
ω	Deposition morphology	
<i>Superscript:</i>		
0	Property of the pristine electrode (without Li_2O_2 precipitation)	
<i>Subscript:</i>		
cat	Cathode	
e	Electrolyte phase	
s	Solid phase	
sep	Separator	

Table S4. Analyzing the experimental response of Li-oxygen porous electrodes³⁹ in near equilibrium conditions. Electrodes have a pristine porosity of 80%, thus a theoretical capacity of 500 mAh/cm².

I_{app} (mA/cm ²)	C-rate	Capacity (mAh/cm ²)	% storage
0.1	C/500	5.99366492	12.0
0.2	C/250	3.68507151	7.5
0.5	C/100	2.13193721	4.3
1	C/50	1.61830077	3.2

References

1. A. N. Mistry and P. P. Mukherjee, *J. Phys. Chem. C*, 2018, **122**, 18329-18335.
2. J. Newman and K. E. Thomas-Alyea, *Electrochemical systems*, John Wiley & Sons, New Jersey, 2012.
3. A. M. Bizeray, D. A. Howey and C. W. Monroe, *J. Electrochem. Soc.*, 2016, **163**, E223-E229.
4. Z. Feng, K. Higa, K. S. Han and V. Srinivasan, *J. Electrochem. Soc.*, 2017, **164**, A2434-A2440.
5. E. Kreyszig, *Advanced Engineering Mathematics*, John Wiley & Sons, Singapore, 2010.
6. L. O. Valøen and J. N. Reimers, *J. Electrochem. Soc.*, 2005, **152**, A882-A891.
7. A. Schürmann, R. Haas, M. Murat, N. Kuritz, M. Balaish, Y. Ein-Eli, J. Janek, A. Natan and D. Schröder, *J. Electrochem. Soc.*, 2018, **165**, A3095-A3099.
8. Z. Ma, X. Yuan, L. Li, Z.-F. Ma, D. P. Wilkinson, L. Zhang and J. Zhang, *Energy Environ. Sci.*, 2015, **8**, 2144-2198.
9. D. A. Porter, K. E. Easterling and M. Sherif, *Phase Transformations in Metals and Alloys, (Revised Reprint)*, CRC press, 2009.
10. A. Mistry, C. Fear, R. Carter, C. T. Love and P. P. Mukherjee, *ACS Energy Lett.*, 2019, **4**, 156-162.
11. M. Avrami, *J. Chem. Phys.*, 1939, **7**, 103.
12. L. Guo, G. Oskam, A. Radisic, P. M. Hoffmann and P. C. Searson, *J. Phys. D: Appl. Phys.*, 2011, **44**, 443001.
13. P. Atkins, J. De Paula and J. Keeler, *Atkins' physical chemistry*, Oxford university press, 2018.
14. W.-J. Kwak, H. Kim, H.-G. Jung, D. Aurbach and Y.-K. Sun, *J. Electrochem. Soc.*, 2018, **165**, A2274-A2293.

15. K. B. Knudsen, T. Vegge, B. D. McCloskey and J. Hjelm, *J. Electrochem. Soc.*, 2016, **163**, A2065-A2071.
16. Z. Liu, P. B. Balbuena and P. P. Mukherjee, *J. Coord. Chem.*, 2016, **69**, 2090-2105.
17. Z. Liu and P. P. Mukherjee, *ACS Appl. Mater. Interfaces*, 2017, **9**, 5263-5271.
18. Z. Liu, L. R. De Jesus, S. Banerjee and P. P. Mukherjee, *ACS Appl. Mater. Interfaces*, 2016, **8**, 23028-23036.
19. A. Torayev, A. Rucci, P. C. M. M. Magusin, A. Demortière, V. De Andrade, C. P. Grey, C. Merlet and A. A. Franco, *J. Phys. Chem. Lett.*, 2018, **9**, 791-797.
20. K.-H. Xue, E. McTurk, L. Johnson, P. G. Bruce and A. A. Franco, *J. Electrochem. Soc.*, 2015, **162**, A614-A621.
21. A. Mistry and P. P. Mukherjee, *J. Phys. Chem. C*, 2017, **121**, 26256-26264.
22. A. N. Mistry, K. Smith and P. P. Mukherjee, *ACS Appl. Mater. Interfaces*, 2018, **10**, 6317-6326.
23. A. N. Mistry, K. Smith and P. P. Mukherjee, *ACS Appl. Mater. Interfaces*, 2018, **10**, 28644-28655.
24. S. Torquato, *Random heterogeneous materials: microstructure and macroscopic properties*, Springer Science & Business Media, 2013.
25. GeoDict (<http://www.geodict.com/>).
26. A. Wiegmann, GEODICT: virtual microstructure simulator and material property predictor (<http://www.geodict.com/>).
27. J. Bao, W. Xu, P. Bhattacharya, M. Stewart, J.-G. Zhang and W. Pan, *J. Phys. Chem. C*, 2015, **119**, 14851-14860.
28. X. Li, *J. Electrochem. Soc.*, 2015, **162**, A1636-A1645.
29. K. Yoo, S. Banerjee and P. Dutta, *J. Power Sources*, 2014, **258**, 340-350.
30. C. P. Andersen, H. Hu, G. Qiu, V. Kalra and Y. Sun, *J. Electrochem. Soc.*, 2015, **162**, A1135-A1145.
31. Y. Wang, Z. Wang, H. Yuan and T. Li, *Electrochim. Acta*, 2015, **180**, 382-393.
32. U. Sahapatombut, H. Cheng and K. Scott, *J. Power Sources*, 2013, **227**, 243-253.
33. Y. Wang and S. C. Cho, *J. Electrochem. Soc.*, 2013, **160**, A1847-A1855.
34. M. Mehta, V. Bevara and P. Andrei, *J. Power Sources*, 2015, **286**, 299-308.
35. A. V. Sergeev, A. V. Chertovich, D. M. Itkis, E. A. Goodilin and A. R. Khokhlov, *J. Power Sources*, 2015, **279**, 707-712.
36. K.-H. Xue, T.-K. Nguyen and A. A. Franco, *J. Electrochem. Soc.*, 2014, **161**, E3028-E3035.
37. C. Jung, T. Zhao and L. An, *J. Power Sources*, 2015, **273**, 440-447.
38. V. Bevara and P. Andrei, *J. Electrochem. Soc.*, 2014, **161**, A2068-A2079.
39. L. D. Griffith, A. E. Sleightholme, J. F. Mansfield, D. J. Siegel and C. W. Monroe, *ACS Appl. Mater. Interfaces*, 2015, **7**, 7670-7678.